Detection of spiral magnetic fields in two flocculent galaxies[*]

J. Knapik[1], **M. Soida**[1], **R.-J. Dettmar**[2], **R. Beck**[3], and **M. Urbanik**[1]

[1] Astronomical Observatory, Jagiellonian University, ul. Orla 171, 30-244 Kraków, Poland
[2] Astronomisches Institut, Ruhr-Universität-Bochum, 44780 Bochum, Germany
[3] Max-Planck-Institut für Radioastronomie, Auf dem Hügel 69, 53121 Bonn, Germany

Abstract. According to the classical axisymmetric dynamo concept, differentially rotating galaxies which lack organized optical spiral patterns and density wave flows should still have spiral magnetic fields with a substantial radial component. To check this hypothesis we observed two flocculent spirals, NGC 3521 and NGC 5055, in the radio continuum (total power and polarization) at 10.55 GHz with a resolution of $1.'13$. A search for traces of optical spiral patterns has also been made by observing them in the Hα line and by filtering their available blue images.

NGC 3521 and NGC 5055 were found to possess a mean degree of magnetic field ordering similar to that in grand-design spirals. However, the polarized emission fills the central region of NGC 5055 while a minimum of polarized intensity was observed in the inner disk of NGC 3521. This can be explained by a more uniform star formation distribution in the centre of NGC 3521, while a higher concentration of star-forming activity in the nuclear region and in the rudimentary spiral "armlets" of NGC 5055 leaves broader interarm regions with unperturbed regular magnetic fields. Both galaxies possess regular spiral magnetic fields with a radial component amounting to 40% – 60% of the azimuthal field. The use of beam-smoothed polarization models demonstrates that this result cannot be produced by limited resolution and projection effects. Furthermore, a large magnetic pitch angle cannot be entirely due to the influence of rudimentary spiral-like features visible in our Hα and enhanced optical images. Thus it appears that the dynamo process is responsible for the radial magnetic field in flocculent galaxies. The measured radial magnetic field component as compared to the azimuthal one is even stronger than predicted by a classical turbulent dynamo which provides arguments in support for modern, non-standard dynamo concepts.

---

1. Introduction

Extensive polarization studies of nearby galaxies revealed the existence of spiral magnetic field configurations with a radial field component comparable in strength to the azimuthal one (Beck et al. 1996). Since strong shearing motions caused by rapid differential rotation will transform any radial structures into azimuthal ones within a few galactic rotations, an effective process continuously regenerating radial magnetic fields is required. The above findings boosted the development of turbulent dynamo theories. According to these, in strongly differentially rotating disks the large-scale radial magnetic field B_r is generated from the azimuthal field B_ϕ according to the equation (in cylindrical galactic coordinates r, ϕ, z, Ruzmaikin et al. 1988):

$$\frac{\partial B_r}{\partial t} = -\frac{\partial}{\partial z}(\alpha B_\phi) + \beta(\Delta \boldsymbol{B})_r \tag{1}$$

while the rotational shear converts B_r back into the azimuthal field:

$$\frac{\partial B_\phi}{\partial t} = r\frac{d\Omega}{dr}B_r + \beta(\Delta \boldsymbol{B})_\phi \tag{2}$$

where $\alpha \propto < \boldsymbol{v} \cdot rot(\boldsymbol{v}) >$ constitutes the measure of mean helicity of a small-scale turbulent velocity field $\boldsymbol{v}$ (also called the α-effect), Ω is the local angular rotation speed of the galactic disk and β is the turbulent diffusion coefficient. The persistence of the radial magnetic field against differential rotation constitutes a typical signature of the dynamo action described by Eq. (1). A vertical magnetic field component is generated as well, however, in realistic dynamo models it becomes significant at $z \geq$ 2–3 kpc (e.g. Urbanik et al. 1997). This is higher than the typical scale height of synchrotron emission of $\simeq 1$ kpc (Hummel et al. 1991), thus vertical fields are usually not seen in emission.

Almost all nearby spiral galaxies known to possess spiral magnetic patterns (Beck et al. 1996) show strong density waves associated with radial gas streaming motions and compression effects. In such objects density wave flows can be at least partly responsible for a strong radial field component and high magnetic pitch angles. In some concepts the non-azimuthal flows in spiral arms may even be a crucial agent for the maintenance of radial magnetic fields (e.g. Otmianowska-Mazur et al. 1997). Thus, the observed radial field component may result from a

complex interplay of density-wave flows and the α-effect (see Moss 1998), difficult to disentangle.

Nearby spirals also have a high concentration of star formation in the spiral arms, which can act destructively on regular magnetic fields in the arms. The specific modulation of kinetic helicity and turbulent diffusion by star formation highly concentrated in spiral arms may strongly influence the global magnetic field structure, too (Rohde et al. 1998, Moss 1998). Thus, the existing data on nearby galaxies does not provide a clear picture of dynamo-generated magnetic fields in a manner free from severe contamination by spiral arms. No observations exist showing the unperturbed dynamo action in differentially rotating galaxies lacking organized spiral arms. The question of whether the spiral-like magnetic fields with a significant radial component can still exist in such objects (which would provide strongest argument for the turbulent dynamo) has remained open up to now. In the opposite case, of B_r being largely due to global radial flows, the magnetic field in the absence of organized spiral arms would be sheared to a purely azimuthal configuration in 1–2 galactic rotations.

In this work we examine the magnetic field properties in two flocculent galaxies lacking strong signatures of density waves, NGC 3521 and NGC 5055. Our aim is to check whether these galaxies show any radial magnetic fields (as predicted by the turbulent dynamo concept) in the absence of systematic, ordered radial flows due to density waves. No existing reliable polarization data for these objects exist in the VLA archives. As the galaxies are angularly large and we are interested in the global, large-scale field geometry rather than in details of their structure, a high sensitivity to weak, smooth, extended polarized emission was required. The 100 m Effelsberg telescope working at 10.55 GHz (to minimize Faraday effects) is a good instrument for this purpose.

Flocculent galaxies (including our program objects) usually possess some relics of a spiral structure in the form of rudimentary "armlets" (seen e.g. in specially filtered near-infrared images, Thornley 1996) or spiral-like star-forming filaments and dust lane segments. (see e.g. optical images of NGC 3521 and NGC 5055 in Sandage 1961). NGC 5055 also shows some spiral-like concentrations of neutral and molecular gas (Thornley & Mundy 1997, Kuno et al. 1997), not accompanied by massive star formation, as usually happens in density-wave galaxies. All such structures are substantially inclined towards the disk centre and thus have quite a large pitch angle. To state definitely that the radial magnetic field component is generated by the dynamo process it is essential to exclude the alternative possibility of its production by local gas streaming and compression along the rudimentary arms, in local "miniature density waves". For this purpose we investigate all possible traces of spiral structure in NGC 3521 and NGC 5055 by means of Hα imaging supplemented by the analysis of available blue light images. Using beam-smoothed polarization models to overcome possible resolution problems (Urbanik et al. 1997) we check to which degree the magnetic field structure and in particular its radial component can be attributed to Hα-emitting, star-forming spiral-like filaments and dust lane segments.

2. Observations and data reduction

2.1. Radio polarization

The total power and polarization observations were performed at 10.55 GHz using the four-horn system in the secondary focus of the Effelsberg 100 m MPIfR telescope (Schmidt et al. 1993). With 300 MHz bandwidth and 40 K system noise temperature, the r.m.s. noise for 1 s integration time and combination of all horns is 2 mJy/b.a. in total power and 1 mJy/b.a. in polarized intensity.

Each horn was equipped with two total power receivers and an IF polarimeter resulting in four data channels containing the Stokes parameters I, Q and U. The telescope pointing was corrected by performing cross-scans of bright point sources at time intervals of about two hours. The flux calibration was performed using the highly polarized source 3C286. A total power flux density at 10.55 GHz of 4450 mJy was adopted using the formulae by Baars at al. (1977). The polarized flux density was calibrated using the same factors as for total power, yielding a degree of polarization of 12.2% for 3C286, which is in good agreement with other published values (Tabara & Inoue 1980).

During the observations 35 coverages of NGC 3521 and 30 of NGC 5055 were collected in the azimuth-elevation frame. The data reduction process was performed using the NOD2 data reduction package (Haslam 1974). By combining the information from appropriate horns, using the "software beam switching" technique (Morsi & Reich 1986) followed by restoration of total intensities (Emerson et al. 1979), we obtained I, Q and U maps for each coverage of a given galaxy. All appropriate maps were then combined using the spatial-frequency weighting method (Emerson & Gräve 1988), followed by a digital filtering process, removing the spatial frequencies corresponding to noisy structures smaller than the telescope beam. Finally the I, Q and U images were combined into the maps of total power, polarized intensity, polarization degree and polarization position angles. Two polarized background point sources, were subtracted from the final I, Q and U maps of NGC 3521 (see Table 2) prior to forming the polarization maps. Their positions and flux densities were estimated using the unpublished VLA B-array map of NGC 3521 kindly supplied by E. Hummel.

2.2. Hα images

The optical observations were performed during four consecutive nights in March 1996 at the 42″ Hall Telescope of the Lowell Observatory at the Anderson Mesa site. The CCD camera used contains a TI 800×800 chip of 15 μm pixels. This results in a field-of-view of about 4.′5 at the f/8 focus with an image scale of 0.″35/pixel. Therefore the objects had to be mapped by three overlapping fields along their major axes. For each position several integrations were taken in a 30 Å filter centered on Hα and in a broad-band R. Integration times typically were 600 sec or 1200 sec in the Hα filter and 120 sec or 300 sec in R. For the central position of each galaxy a short exposure of only 20 sec was taken in the broad-band filter to avoid saturation of the bright nucleus.

Table 1. Basic properties of NGC 3521 and NGC 5055 (from the Lyon-Meudon Extragalactic Database)

	NGC 3521	NGC 5055
Other names	PGC 33550	PGC 46153, M63
R.A.$_{1950}$	$11^h 03^m 15^s.1$	$13^h 13^m 39^s.9$
Decl.$_{1950}$	$0°13'58''.1$	$42°17'55''.0$
R.A.$_{2000}$	$11^h 05^m 48^s.9$	$13^h 15^m 49^s.2$
Decl.$_{2000}$	$-0°02'14''.7$	$42°02'05''.9$
Inclination*	$64°$	$55°$
Position Angle	$163°$	$105°$
Morphol. Type	SBbc	Sbc
Distance [Mpc]	$7.2**$	$7.2**$
Optical diameter D$_{25}$	$10'.7$	$13'.0$

* $0°$ = face-on

** Tully (1988)

Since the observations were made under relatively bad seeing conditions, the individual images were binned by a factor of two after standard reduction of the frames without loss of information. Overlapping fields were combined by aligning them with reference to stars or bright knots in the overlap regions and by scaling them by exposure time after removal of the varying night sky contribution. In combining the individual frames an appropriate filter was used to avoid the inclusion of saturated pixels. The continuum contribution to the intensity in the Hα filter was removed by subtracting a scaled version of the R filter. Finally, the coordinate system for the resulting Hα map was obtained from a comparison with stars from the ST-GSC[1].

3. Observational results

The Hα emission of NGC 3521 lacks evident signs of spiral structure. The eastern side of the disk is flanked by a chain of HII regions extending towards the north along a pair of weak mutually crossing arms. The total power map of NGC 3521 with superimposed B-vectors of polarized intensity overlaid upon the Hα data is presented in Fig. 1. The galaxy shows a bright radio disk with some extension along the peculiar dust lane in the SW disk, visible also in the map of Urbanik et al. (1989) and of Condon (1987). It is not associated with any Hα-emitting structures thus it cannot be caused by local star-forming processes. The map of polarized intensity (Fig. 2) shows two separate polarized regions, extending along the disk boundary and shifted clockwise from the minor axis. The observed B-vectors are roughly parallel to the faint optical spiral-like features and dust lanes. The SE part of the polarization map is strongly affected by confusing sources and should be considered with care.

The integration of maps of the total power and polarized intensity of NGC 3521 in elliptical rings with an inclination of $64°$ and a position angle of $163°$ yields the 10.55 GHz total power flux density of 86 ± 12 mJy within the radius of $7'$ and the polarized flux density of 2.1 ± 1.1 mJy within $6'$. This implies a mean polarization degree of $2.4 \pm 1.3\%$.

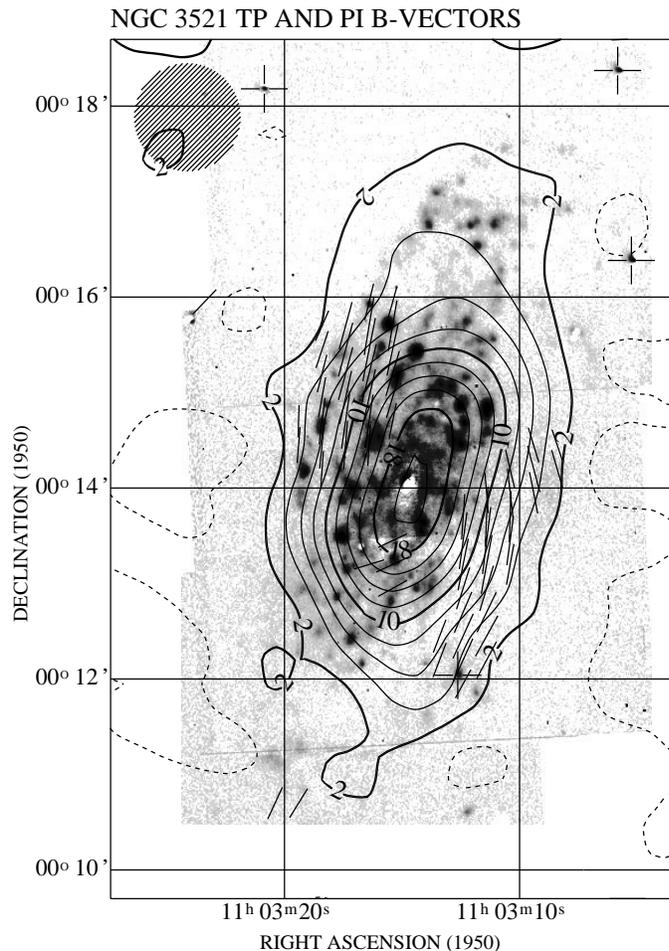**NGC 3521 TP AND PI B-VECTORS**

Fig. 1. The total power contour map of NGC 3521 with superimposed vectors of polarized intensity, both at the original resolution of $68''$, overlaid onto the Hα image. The contour levels are plotted every 2 mJy/b.a.. The r.m.s. noise is 0.6 mJy/b.a. so the first contour corresponds to about 3.5σ

Table 2. Background sources removed from the radio maps of NGC 3521

	source No. 1	source No. 2
R.A.$_{1950}$	$11^h 03^m 22^s.70$	$11^h 03^m 19^s.19$
Decl.$_{1950}$	$0°12'15''.0$	$0°12'47''.0$
Flux density at 10.55 GHz	13.1 mJy	13.1 mJy
Degree of polarization	18%	11%
Pol. position angle	$15°$	$30°$

The Hα map of NGC 5055 shows weak traces of spiral structure in the form of aligned chains of HII regions in the SE disk and west of the centre. The total power map (Fig. 3) shows a bright central region which is only barely resolved with our beam and a weaker radio envelope. The polarized intensity in NGC 5055 (Fig. 4) forms a broad lobe extending along the minor axis through the disk centre with a long extension to the NW. The magnetic vectors are mostly parallel to the major axis.

The integration of the total power map of NGC 5055 was performed in elliptical rings with an inclination of $55°$ and a
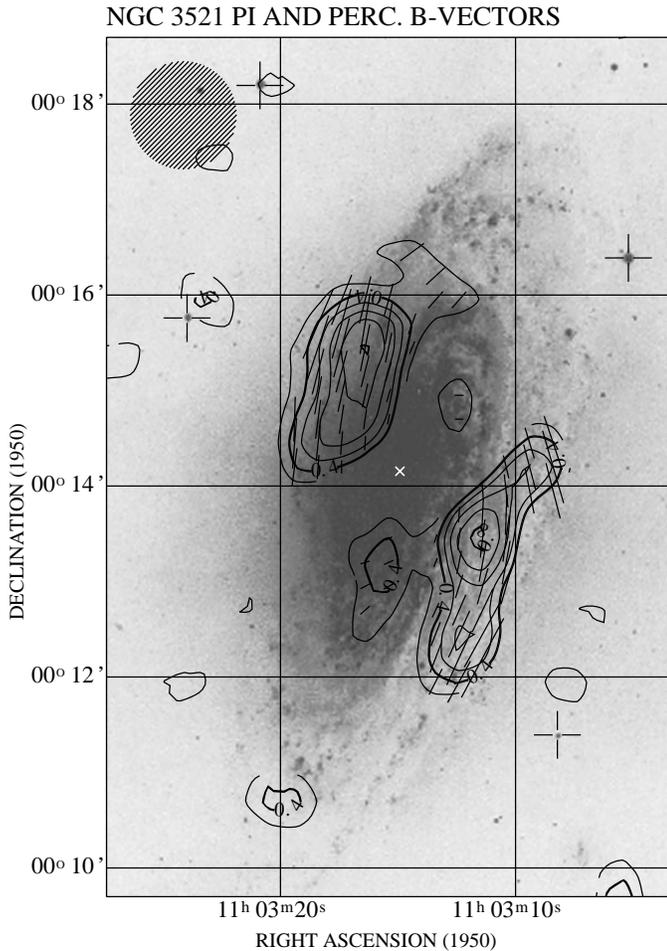
NGC 3521 PI AND PERC. B-VECTORS

Fig. 2. The contour map of the polarized intensity of NGC 3521 with vectors of polarization degree, both at the original resolution of 68″, overlaid onto the digitally enhanced blue light optical image from the "Carnegie Atlas of Galaxies" (Sandage & Bedke 1994). The contour levels are plotted from 0.3 mJy/b.a. with step 0.1 mJy/b.a.. The r.m.s. noise is 0.14 mJy/b.a. so the first thick, labelled contour corresponds to about 3σ. The cross denotes the galaxy's centre as measured from our red map

position angle of 105° (see Table 1). It yields the total power flux density at 10.55 GHz of 83 ± 13 mJy within a radius of 7′ (similar to the value obtained by Niklas et al. 1995), and the polarized flux density of 4.2 ± 1.5 mJy inside 3′.5. This implies a mean polarization degree of $5.0 \pm 2.5\%$.

4. Discussion

4.1. Global galaxy parameters

The surface brightness of both galaxies at 10.55 GHz implies mean equipartition total magnetic field strengths of about 10.5 μG for NGC 3521 and 9.2 μG for NGC 5055, assuming a total face-on thickness of the radio disk of 2 kpc, a lower energy cutoff for relativistic electrons of 300 MeV and a proton to electron energy density ratio of 100. For NGC 5055 we used a spectral index of -0.79 computed from our and Con-

don's (1987) measurements. The same value was adopted for NGC 3521, as no lower-frequency data corrected for confusing sources are so far available. The computed field strengths are comparable to those of radio-bright nearby spirals (Beck et al. 1996), thus the lack of organized spiral arms apparently does not lead to significantly weaker magnetic fields.

Fig. 5 compares the mean polarization degree at 10.55 GHz of NGC 3521, NGC 5055 and of grand-design spirals as a function of their star formation efficiency (as estimated crudely by the mean surface brightness at 60 μm taken from IRAS catalogues, Lisenfeld et al. 1996). We expect that galaxies of various linear sizes develop the global magnetic field with structures closing on scales proportional to the galaxy dimensions. To ensure the same degree of beam depolarization with respect to galaxy-scale field structures we convolved their U and Q maps to the same beam size relative to the optical diameter.

Although the polarized emission avoids regions of high star formation inside individual galaxies (see Beck et al. 1996) there is no general relationship between the mean 60 μm surface brightness and the integrated degree of polarization (except some deviation exhibited by M83, Fig. 5). The degree of polarization of the latter galaxy may be somewhat enhanced due to the magnetic field alignment along the bar (see Beck et al. 1999) or local gas compressions, seen on high contrast images as a network of sharp dust lanes filling the whole disk (Malin priv. comm.). Apart from this object there is no general trend of IR brighter spirals being more polarized. We checked these findings for a possible bias due to different galaxy inclinations: no obvious correlation between the polarization degree and the inclination was found.

NGC 5055 has a polarization degree higher than some grand-design spirals and nearly the same as NGC 4254 (see Soida et al. 1996), which belongs to the strongest polarized spirals after M83. NGC 3521 is the least polarized object in our sample, however its polarization degree is only a factor of 0.7 lower than that of the strong density-wave, similarly inclined object NGC 3627 (Soida et al. 1999). Taking into account the errors of polarization degree, the flocculent galaxies studied in this work do not seem to possess a systematically lower degree of magnetic field ordering than that in grand-design galaxies, which could be attributed to a lack of organized spiral arms. *A strong density wave action is apparently not an important agent in producing strong regular magnetic fields.*

Fig. 6 compares the radial distributions of polarized intensity and Hα brightness for the studied galaxies. Both objects have (to the limits of errors) a similar polarized brightness beyond 0.2 of the optical radius R$_{25}$. However, while the polarized brightness continues to rise towards the centre in NGC 5055, it drops suddenly in the inner disk of NGC 3521. This is accompanied by differences in the distribution of Hα brightness. The Hα emission in NGC 5055 is highly concentrated in the nuclear region while in NGC 3521 it forms a broad "plateau" extending up to 0.3 R$_{25}$. Moreover, while star-forming processes traced by the Hα emission fill the inner disk of NGC 3521 more uniformly, they are more concentrated in the arm-like chains of HII regions in NGC 5055. This implies more efficient destruction of
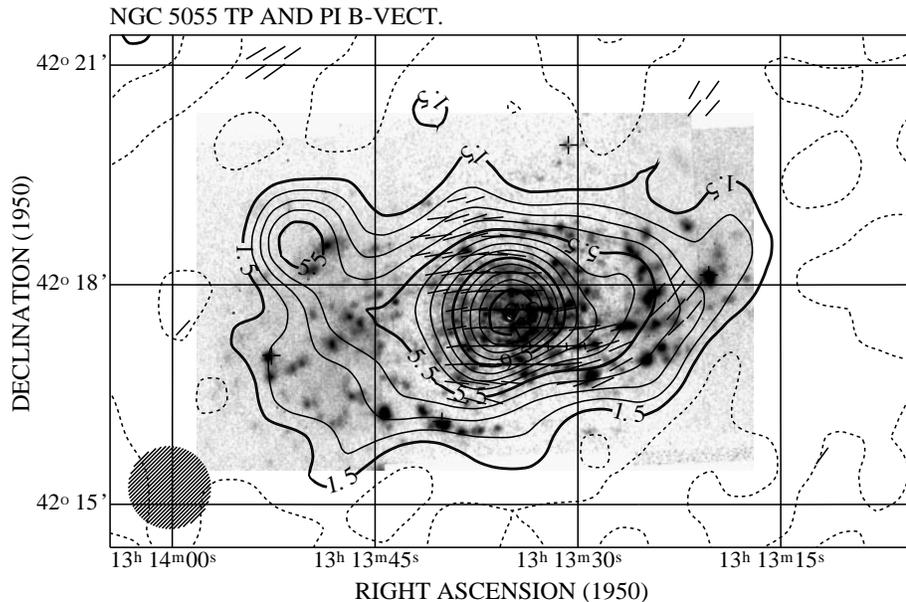
NGC 5055 TP AND PI B-VECT.

Fig. 3. The total power contour map of NGC 5055 with superimposed vectors of polarized intensity, both at the original resolution of 68″, overlaid onto the Hα image. The contour levels are plotted from 1.5 mJy/b.a. with step 1.0 mJy/b.a.. The r.m.s. noise is 0.6 mJy/b.a. so the first contour corresponds to about 3σ
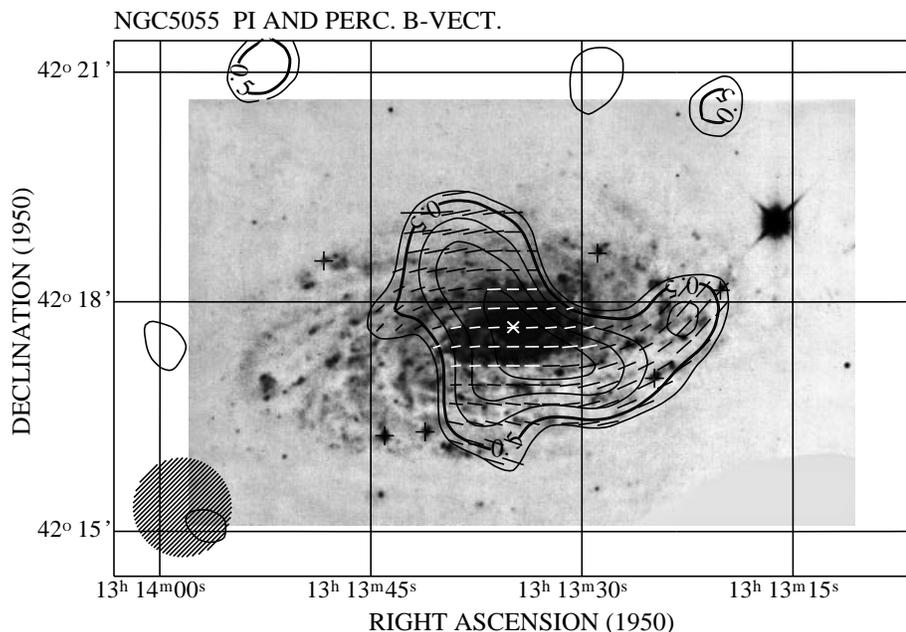
NGC5055 PI AND PERC. B-VECT.

Fig. 4. The contour map of the polarized intensity of NGC 5055 with vectors of polarization degree, convolved to a beam of 1′3 overlaid onto the digitally enhanced optical image from the "Carnegie Atlas of Galaxies" (Sandage & Bedke 1994). The contour levels are plotted from 0.4 mJy/b.a. with step 0.1 mJy/b.a.. The r.m.s. noise is 0.14 mJy/b.a. so the first thick, labelled contour corresponds to about 3σ. The cross denotes the galaxy's centre as measured from our red map

regular fields in the inner disk of NGC 3521 by supernova explosions, stellar winds etc., which gives rise to a central depression in the polarized emission. We suspect that the polarized surface brightness of the galactic disk may depend more on the star formation *distribution* rather than on the overall star-forming activity. Even rapidly star-forming galaxies may show highly polarized emission if star formation is strongly concentrated in spiral arms, leaving broad, quiet interarm regions with highly ordered magnetic fields.

4.2. Structure of large-scale magnetic fields

Fig. 7 shows the distribution of polarized intensity and the orientation of B-vectors as a function of azimuthal angle in the disk plane and the natural logarithm of the galactocentric radius.

In such coordinates a logarithmic spiral appears as a straight line with an inclination equal to its pitch angle. As such graphs are subject to strong beam smearing effects in central regions, Fig. 7 is calculated for galactocentric radii $r \geq 1'$. The region of NGC 3521 between the azimuthal angles of 180° and 240° and $\ln(r) < 0.5$ is confused by the background source and we excluded it from considerations.

In both galaxies the magnetic pitch angles ψ differ significantly from zero, their mean absolute values are 31° ± 4° in NGC 3521 and 24° ± 4° in NGC 5055, thus on average the observed radial magnetic field component constitutes respectively 60% and 42% of the azimuthal component. In specific polarized lobes the mean pitch angles are: in NGC 3521 39° ± 5° in the NE lobe and 25° ± 5° in the SW one, in NGC 5055 we obtained 23° ± 5° in the northern and NE disk and 26° ± 5°
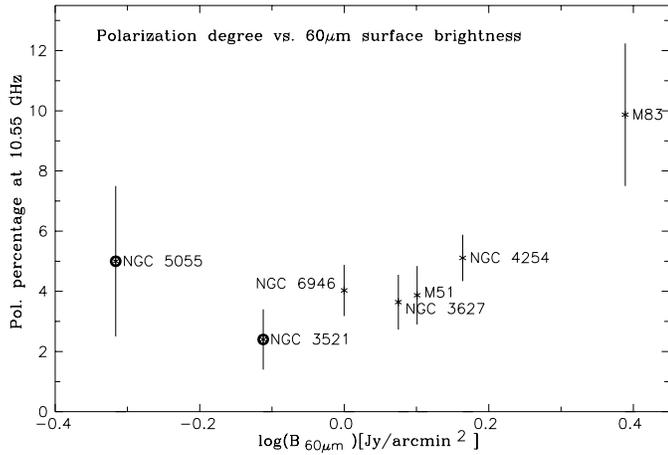
Fig. 5. A comparison of the mean polarization degree of NGC 3521, NGC 5055 and nearby grand-design spirals as a function of 60 μm surface brightness. Before combining the U and Q data into the maps of polarized intensity they were convolved to the same beam relative to the galaxy's optical radius, in order to ensure the same degree of beam depolarization with respect to their global magnetic field structures. The U and Q maps are taken from the MPIfR archives of Effelsberg polarization data. The 60 μm surface brightness is computed by dividing the IRAS flux by the face-on corrected disk area within the isophote of $25^m/(\square'')$

Fig. 6. a Radial distributions of polarized intensity of NGC 3521 and NGC 5055 integrated in rings with inclinations and major axis orientations as in Table 1. The same rings $20''$ wide are used for both galaxies since for the radio data the degree of data smearing is determined by the beamsize. **b** Radial distributions of the Hα brightness integrated in rings with orientation parameters from Table 1. Each Hα profile is normalized to its maximum value. To ensure the same degree of data smearing relative to the optical diameter, in this case we used a ring width of $20''$ for NGC 3521 and $24''.1$ for NGC 5055. In both graphs the galactocentric radius is normalized to the optical disk radius at the level of $25^m/(\square'')$ taken from the LEDA database (see Table 1)

in southern and SW disk. In each galaxy the polarized intensity peaks are placed symmetrically on both sides of the disk but shifted in azimuth from the minor axis according to the sign of the pitch angle of magnetic vectors. The azimuthal angle of the shift is similar to the mean pitch angle. This shift constitutes a geometrical effect caused by a non-zero radial magnetic field (see Urbanik et al. 1997) and provides further evidence for the existence of a radial field component.

We checked the above findings for possible effects of our limited resolution and the influence of vertical magnetic fields projected onto the sky plane in rather highly inclined objects. For this purpose we used beam-smoothed polarization models based on three-dimensional dynamo-generated fields with a strong vertical component, selected from a large library of dynamo results prepared by D. Elstner in course of modeling works described by Urbanik et al. (1997). A number of models were computed with various intrinsic magnetic pitch angles. Obtaining the dynamo-generated magnetic fields with a given (especially large) pitch angle by solving the dynamo equations numerically requires extremely elaborate calculations. Our aim was only to check for possible biases introduced by resolution and projection effects rather than fitting concrete physical dynamo models to our data, thus it was sufficient to regulate the intrinsic magnetic pitch angle by multiplying the toroidal field strength in the chosen model by a constant factor. A reference model containing pure azimuthal field was computed as well. The models of polarized emission smoothed to the beam of $1'.13$ were obtained by integrating Stokes I, Q and U parameters as described by Urbanik et al. (1997). Separate models were computed for NGC 3521 and NGC 5055, taking into account their
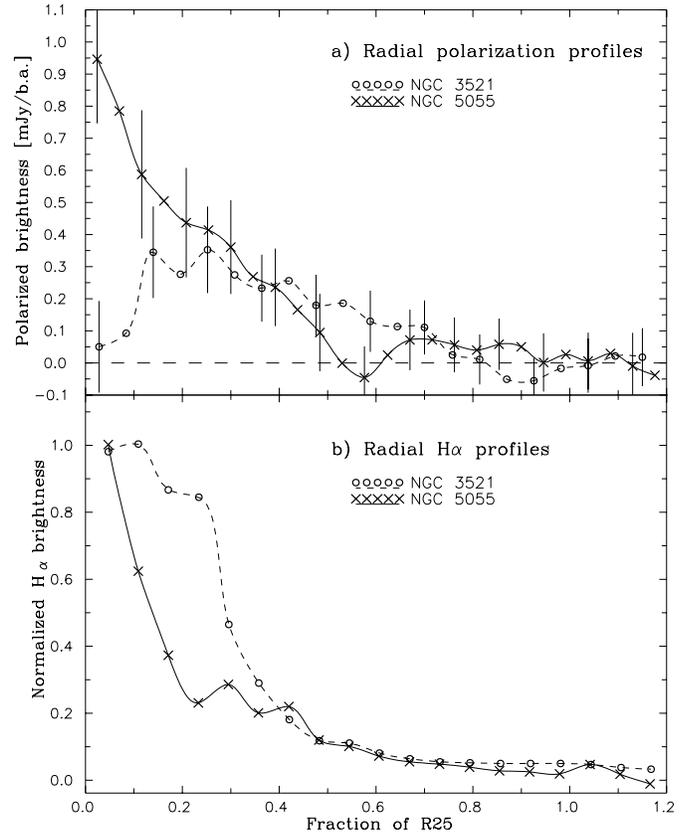
inclinations from Table 1 and the fact that the central region of NGC 3521 is unpolarized while in NGC 5055 the polarized emission fills the whole inner disk. The radial exponential scale length of CR electron density was adjusted to reproduce the radial distribution of polarized intensity. In the z-direction a Gaussian relativistic electron density distribution with a scale height of 1 kpc was adopted. The simulated maps of polarized intensity were analyzed in the azimuth $-\ln(r)$ frame in the same way as those of observed galaxies.

Results displayed in Fig. 8a demonstrate that purely azimuthal fields can generate some inclined B-vectors. However, their pitch angles are of opposite sign and of the same absolute value on both sides of each lobe. The B-vectors are perfectly azimuthal inside the polarized lobes, which are always peaking at the minor axis. This behaviour results from the geometry of the azimuthal field, whose projection is always symmetrical with respect to the minor axis, with the maximum of the regular
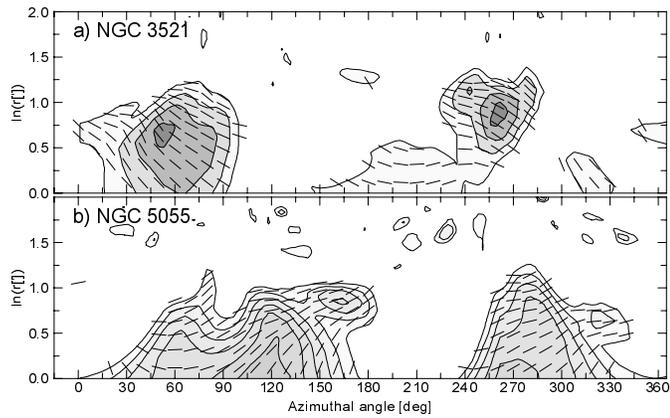
Fig. 7a and b. Plot of the distribution of polarized intensity (contours and greyscale) and of the orientations of polarization B-vectors in the azimuth - $\ln(r)$ frame (r is the galactocentric radius in arcmin) for NGC 3521 **a** and NGC 5055 **b**. The azimuthal angle runs anticlockwise from the northern part of the major axis in NGC 3521 and from the western part of the major axis in NGC 5055

Fig. 8a–c. Plot of the distribution of polarized intensity (contours and greyscale) and of the orientations of polarization B-vectors in the azimuth – $\ln(r)$ frame (r is the galactocentric radius in arcmin) for axisymmetric model containing only azimuthal magnetic field **a**, for the dynamo-type magnetic field with regular component in the central region suppressed to reproduce the polarization minimum in NGC 3521 **b**, and for the case of NGC 5055 with dynamo-type regular fields extending to the disk centre **c**. In cases **b** and **c** we used a combination of poloidal and toroidal magnetic fields resulting from the numerical dynamo simulations by D. Elstner showing a strong vertical component, with the ratio of poloidal to toroidal fields adjusted to yield the pitch angles of B-vectors similar to those in real galaxies. The models are convolved to a beam of $1.'13$

field perpendicular to the line of sight ($B_\perp$) falling exactly at the minor axis. A non-zero pitch angle of the same sign throughout the whole polarized lobes can be obtained only when a poloidal (thus also radial) magnetic field is allowed (Fig. 8b and c). Only in this case it was possible to obtain a shift of polarized intensity maxima from the minor axis, resulting from the geometry of magnetic lines. If a radial magnetic field component is added, making the magnetic lines deviate from the azimuthal direction by a given pitch angle ψ, the maximum $B_\perp$ occurs at an azimuthal distance from the minor axis roughly equal to ψ, as can be seen in Fig. 8b and c (see also Urbanik et al. 1997).

If the regular magnetic field in the central region is suppressed, no radially directed B-vectors are obtained (Fig. 8b). If regular fields extend to the centre, the groups of radial B-vectors occur close to azimuthal angles of $0°$ and $180°$, thus running across the centre along the major axis. This picture agrees well with Fig. 7a (no radial fields observed in NGC 3521) and b (radial magnetic fields in NGC 5055 especially obvious at azimuthal angles $0° – 30°$). In the latter case our model reproduces well the characteristic pitch angle reversal in the mentioned range of azimuthal angles. There is thus no need to invoke any bisymmetric fields to explain the B-vectors crossing the central region in NGC 5055.

Table 3 compares the mean intrinsic magnetic pitch angles for the whole series of adopted model magnetic fields with those measured from a beam-smoothed polarization model. As in dynamo models the intrinsic pitch angle changes with the distance from the disk plane z, the observed values of ψ depend on the vertical CR electron distribution. To account for this effect and to single out effects of projection and resolution the intrinsic pitch angles were averaged, weighting them with the assumed vertical distribution of CR electron density. The observed pitch angles of B-vectors were averaged over each polarized lobe in the Stokes QU plane (as the radio telescope does).
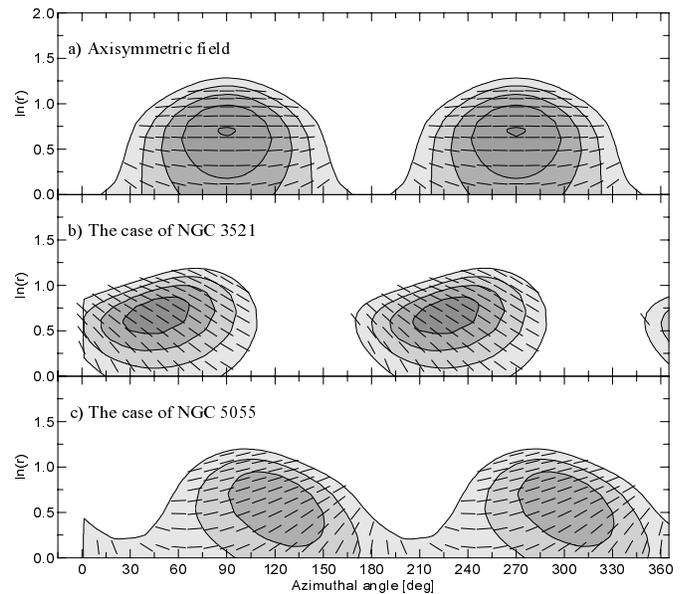
For observed pitch angles smaller than $40°$ (as found in NGC 3521 and NGC 5055) there is almost perfect agreement between assumed and measured values of ψ. For larger pitch angles, the beam-smoothed values become higher than the assumed values by a few degrees. The differences become large for observed pitch angles greater than $60°$. The effect is due to an increasing role of the poloidal magnetic field with respect to the azimuthal field which also causes a greater contribution of the sky-projected, beam-smoothed vertical field component. It follows from Table 3 that the intrinsic magnetic pitch angle in both galaxies cannot be significantly smaller than the observed values. In particular, the resolution and projection effects are unable to produce the observed radial fields out of purely azimuthal ones.

4.3. Traces of spiral structure and the origin of magnetic fields

Using our Hα maps and the digitally enhanced blue optical images (Fig. 9) of NGC 3521 and NGC 5055 we are able to trace weak signs of spiral structure. Though both galaxies exhibit similar traces of a spiral pattern in the near-infrared (Thornley 1996), NGC 3521 shows only weak signs of spiral structure in its
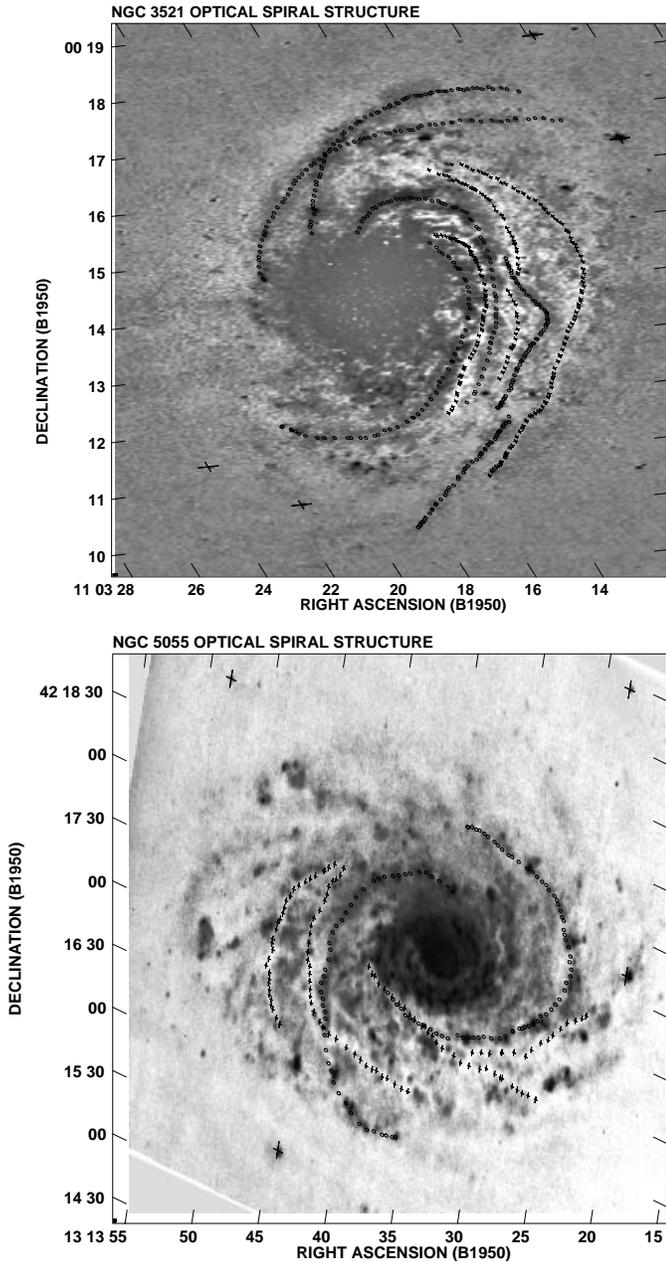
Table 3. A comparison of intrinsic magnetic pitch angles to those measured from beam-smoothed polarized intensity maps

model	intrinsic $\psi[°]$	measured $\psi[°]$
1	0.3	0.2
2	2.7	2.4
3	12.7	12.1
4	22.3	23.1
5	33.8	40.5
6	45.6	64.9
7	50.0	77.8

Fig. 9. The face-on deprojected, digitally filtered and enhanced blue optical images of NGC 3521 (upper panel) and NGC 5055 (lower panel), showing faint spiral structures. The most prominent structures were marked by symbols – optically bright "armlets" by circles and dust features by crosses

detectable density-wave signs described by Thornley & Mundy (1997) and by Kuno et al. (1997). The weak infrared arms discussed by Thornley & Mundy (1997) correspond to two aligned chains of HII regions seen in our Hα map. Using both the Hα and optical images we traced them out to a further distance than Thornley & Mundy (1997). In the enhanced optical image we identified also several spiral-like dust lanes (Fig. 9).

To check for possible associations between the magnetic field orientations and those of star-forming filaments and dust lanes we again used the beam-smoothed models of polarized emission obtained by integrating the U and Q Stokes parameters due to an assumed magnetic field structure. The regular fields were assumed to be locally parallel to rudimentary spiral-like features shown in Fig. 9 and distributed in a way yielding the observed distribution of polarized intensity.

In NGC 3521 the mean modeled pitch angle is in both lobes smaller by about 3σ errors than the observed one (Fig. 10). The observed values of ψ higher than the modeled ones occur in almost all individual map points which have the observed polarized intensity above the noise level, the differences reach locally $30°$ ($\geq 6\sigma$). In the southern and SW disk of NGC 5055 (azimuths $30° - 150°$) no systematic difference between mean modeled and observed magnetic pitch angles has been found. However, in the NE disk (the azimuthal angle range $180° - 360°$) the model yields small pitch angles in agreement with a preponderance of nearly azimuthal optical structures, while the observed mean value of ψ is much higher, similar to that in the SW lobe (Fig. 10), as expected for an axisymmetric turbulent dynamo. We also stress that NGC 3521 while possessing much weaker signs of organized spiral structure does not show smaller mean pitch angles of polarization B-vectors than NGC 5055, as one could expect if the radial magnetic field were primarily due to local radial flows and/or compressions in arm-like spiral structures. In the face of the above, the radial magnetic fields and large pitch angles are unlikely to be caused by gas flows and compressions in spiral features and need to be explained by a turbulent dynamo process.

Though the dynamo action generates primarily radial fields, too high magnetic pitch angles can make a problem for the classical dynamo concept. The analysis of mathematical properties of Eqs. (1) and (2) by Ruzmaikin et al. (1988) implies that for
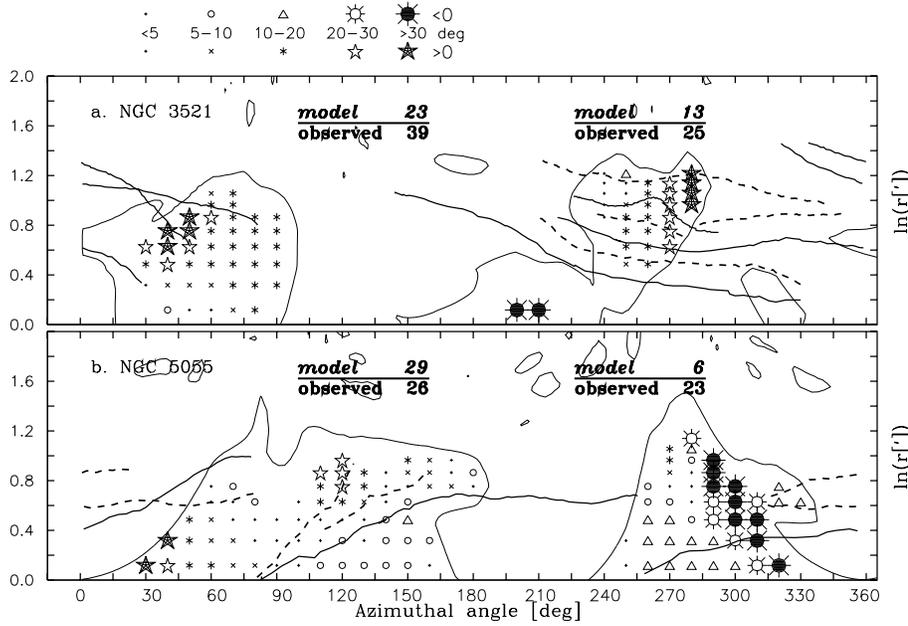
Hα emission. The inner disk is filled uniformly with chaotically distributed HII regions, the NE arm seen by Thornley (1996) is composed of two mutually crossing segments having different pitch angles (Fig. 9). Aligned Hα structures are found only close to the inner part of one segment NE and east of the centre. No aligned Hα structures accompany the dust lanes and total power ridge on the western and SW disk side.

Generally NGC 5055 seems to show a better degree of alignment of Hα and optical features, in agreement with weak but still

Fig. 10a and b. The azimuth - $\ln(r)$ plot of differences between observed magnetic pitch angles in NGC 3521 **a** and NGC 5055 **b**, and those obtained for models assuming a magnetic field aligned with optically bright armlets and dust lanes, as marked in Fig. 12 but having the same polarized intensity distribution as observed. Various symbols denote particular intervals of these differences (see the figure legend). Pitch angles are computed within the second contour given in Fig. 8, for comparison the outline of the first contour is plotted as well. The dust lanes (dashed lines) and optically bright "armlets" (solid lines) are also shown. The error of pitch angles is about $5°$ in the inner part of polarized lobes and about $7°$ in their outer regions, rising to about $9°$ in polarized extensions stretching to the right of main lobes in NGC 5055. The numbers near the top of each panel show the mean pitch angles: modeled (top line) and observed, both averaged over particular polarized lobes

differentially rotating galaxies (to which both discussed objects belong, Burbidge et al. 1960, 1964):

$$\frac{B_r}{B_\phi} = \left(\frac{\beta^2}{\alpha_0 \Omega_0 h_0^3}\right)^{1/2} \tag{3}$$

where α_0 and Ω_0 are the typical values of α and Ω in the disk, while h_0 is the scale height of ionized gas. These authors define the dynamo number D measuring the dynamo efficiency as $D = \alpha_0 \Omega_0 h_0^3 / \beta^2$. As the ratio B_r/B_ϕ defines the magnetic pitch angle ψ Eq. (3) implies that:

$$\tan \psi = |D|^{-1/2} \propto 1/(\alpha_0 \Omega_0)^{1/2} \tag{4}$$

Thus, the stronger the dynamo action the smaller is the magnetic pitch angle. This is largely due to the fact that the kinetic helicity α driving the dynamo depends primarily on the turbulence vorticity $< rot(\boldsymbol{v}) >$ which is driven by Coriolis forces proportional to the angular disk speed Ω, hence $< rot(\boldsymbol{v}) >$ and α are proportional to Ω, as well. A strong dynamo action requires a high degree of turbulence helicity, and thus rapid rotation. As normal galaxies mostly rotate differentially, this in turn leads to a faster conversion of the radial field component into the azimuthal one (Eq. (2)) thereby decreasing the magnetic pitch angle. By all the above *large magnetic pitch angles* need a *weak dynamo action* with a slow rotation and/or a small α yielding together a small absolute value of the dynamo number $|D|$ (Eq. (4)).

The dynamo number D cannot be arbitrarily decreased to produce large magnetic pitch angles. Solutions of Eqs. (1) and

(2) are sought in the form $B_{r,\phi}(t) = B_{r,\phi}^0 e^{-\gamma t}$. The magnetic field generation requires its growth with time and hence a positive value of the growth rate γ. This parameter is an increasing function of the absolute value of dynamo number D (Ruzmaikin et al. 1988). For $|D|$ smaller than some critical value $|D_{cr}|$ γ is negative and the magnetic field decays. An efficient field amplification needs $|D| >> |D_{cr}|$. The latter quantity depends on many detailed assumptions concerning e.g. the distribution of α with the height above the disk etc. but for realistic galaxy models $|D_{cr}|$ cannot be lower than $\simeq 6$–10. For this reason classical dynamo models have problems with generating spiral-like magnetic fields with pitch angles in excess of $17° - 20°$. The above formalism applied to mean magnetic pitch angles of observed galaxies implies the mean dynamo numbers $|D| \approx 2.8$ in NGC 3521 and $|D| \approx 4.5$ in NGC 5055, considerably below the required 6–10 for normal spiral galaxies (Ruzmaikin et al. 1988). Taking into account all uncertainties and approximations, the classical dynamo process in the studied galaxies would at best work at its critical threshold. With γ of about zero or just above it the production of galaxy-scale magnetic fields would be extremely slow and inefficient, if possible at all.

More recent, refined numerical dynamo models, involving a feedback of magnetic fields upon turbulent motions (e.g. Elstner et al. 1996) encounter a similar pitch angle problem. The above authors found that, in the case of an axisymmetric dynamo, large pitch angles require large turbulence correlation times (see Elstner et al. 1996 for detailed definitions), which in turn gives rise to oscillatory, dipole solutions, very unlikely to exist in real

galactic disks. Rohde & Elstner (1998) attained a steady dynamo solution with pitch angles reaching $40°$ in case of turbulence modulation by star formation enhancement in spiral arms. However, the applicability of this model to flocculent galaxies having little concentration of star-forming processes in spiral arms (as shown by our Hα images) is highly disputable. The very recent, non-standard models of dynamo driven by magnetic buoyancy (Moss et al. 1999) are more promising. The quoted authors obtained typical magnetic pitch angles of order $30°$, they also obtained reasonable solutions with B_r comparable to B_ϕ. Our observations of quite large pitch angles of B-vectors apparently support these new dynamo concepts.

Another problem with applying the dynamo concept to flocculent galaxies is the magnetic pitch angle asymmetry in NGC 3521. In normal galaxies the dynamo process generates an axisymmetric magnetic field with a similar mean pitch angle in both polarized lobes (Fig. 8) as indeed observed in NGC 5055. In contrast, in NGC 3521 both polarized lobes differ in the magnetic pitch angle ψ by more than 3σ r.m.s. error, which cannot be explained by the axisymmetric dynamo. We note however, that smaller values of ψ in the SW disk are associated with smaller optical pitch angles and that this region also contains a total power ridge not caused by local star-forming processes (Sect. 3). Moreover, the analysis of the red optical image by Dettmar & Skiff (1993) suggests that this region might recently have been perturbed by a "soft merging" event or compressions by the intergalactic gas in which case the total power ridge might result from the magnetic field squeezing. As the pitch angle decrease on the compressed side has been observed in wind-swept galaxies NGC 4254 (Soida et al. 1996) and NGC 2276 (Hummel & Beck 1995), the same sort of interactions may explain the pitch angle asymmetry in NGC 3521.

5. Summary and conclusions

In order to check whether galaxies lacking organized optical spiral patterns still possess spiral magnetic fields, we mapped two flocculent galaxies showing only weak signs of global spiral structures in total power and polarization at 10.55 GHz. A single-dish instrument, the 100 m Effelsberg telescope, was used to obtain maximum sensitivity to weak extended emission. The most important results are as follows:

- Both galaxies have a mean degree of magnetic field regularity not significantly lower than that of a small sample of grand-design spirals with similar star-forming properties. Some differences in the polarized emission from the central regions of observed flocculent spirals may be explained by differences of the star formation distribution in their inner disks
- Despite a lack of obvious density wave action both flocculent objects show spiral-like regular magnetic fields with a significant radial component as expected for the dynamo action. The mean magnetic pitch angles in both galaxies are similar and amount to some $25° - 30°$, being somewhat larger in NGC 3521. Beam-smoothed polarization models were applied to prove that such large pitch angles cannot

constitute an artifact of limited resolution and projection effects
- The magnetic pitch angles are only loosely connected to those of rudimentary optical structures and are likely caused by turbulent dynamo action. However, such large pitch angles pose some problems to classical dynamo theory, preferring newly developed non-standard dynamo concepts

In this work we demonstrate for the first time that flocculent galaxies are able to develop regular spiral magnetic fields similar in strength and structure to those in grand-design spirals, thus *large-scale density-wave flows are not needed to produce global spiral magnetic fields with a substantial radial component*. We believe that this provides arguments in support of the existence of turbulent dynamo action, free from effects of density wave flows, making it difficult to single-out pure dynamo-type magnetic fields in nearby spirals. To make the dynamo possible an efficient turbulent diffusion of the magnetic field is required rather than the often assumed nearly perfect flux freezing. However, details of the magnetic field properties may depend on the distribution of star-forming processes. We think that our present results make flocculent galaxies worth observing at higher resolution, to clarify the details of the magnetic field properties.

References

Baars J.W.M., Genzel R., Pauliny-Toth I.I.K., Witzel A., 1977, A&A 61, 99

Beck R., Brandenburg A., Moss D., Shukurov A., Sokoloff D., 1996, ARA&A 34, 155

Beck R., Ehle M., Shoutenkov V., Shukurov A., Sokoloff D., 1999, Nat 397, 324

Burbidge E.M., Burbidge G.R., Crampin D.J., Rubin V.C., Prendergast K.H., 1964, ApJ 139, 1058

Burbidge E.M., Burbidge G.R., Prendergast K.H., 1960, ApJ 131, 282

Condon J.J., 1987, ApJS 65, 485

Dettmar R-J, Skiff B.A., 1993, In: The Evolution of Galaxies and Their Environment. NASA Ames Research Center, p. 251

Elstner D., Ruediger G., Schultz M., 1996, A&A 306, 740

Emerson D.T., Gräve R., 1988, A&A 190, 353

Emerson D.T., Klein U., Haslam C.G.T., 1979, A&A 76, 92

Haslam C.G.T., 1974, A&AS 15, 333

Hummel E., Beck R., Dahlem M., 1991, A&A 248, 23

Hummel E., Beck R., 1995, A&A 303, 691

Kuno N., Tosaki T., Nakai N., Nishiyama K., 1997, PASJ 49, 275

Lisenfeld U., Völk H.J., Xu C., 1996, A&A 306, 667

Morsi H.W., Reich W., 1986, A&A 163, 313

Moss D., 1998, MNRAS 297, 860

Moss D., Shukurov A., Sokoloff D., 1999, A&A 343, 120

Niklas S., Klein U., Wielebinski R., 1995, A&A 293, 56

Otmianowska-Mazur K., von Linden S., Lesch H., Skupniewicz G., 1997, A&A 323, 56

Rohde R., Elstner D., 1998, A&A 333, 27

Rohde R., Elstner D., Rüdiger G., 1998, A&A 329, 911

Ruzmaikin A.A., Shukurov A.M., Sokoloff D.D., 1988, Magnetic Fields of Galaxies. Ap&SS Library Vol. 133, Kluwer Academic Publishers

Sandage A., 1961, The Hubble Atlas of Galaxies. Carnegie Inst. of Washington, Washington D.C.

Sandage A., Bedke J., 1994, The Carnegie Atlas of Galaxies. Carnegie Ins. of Washington with The Flintridge Foundation, Washington D.C.

Schmidt A., Wongsowijoto A., Lochner O., et al., 1993, MPIfR Technical Report No. 73, MPIfR, Bonn

Soida M., Urbanik M., Beck R. 1996, A&A 312, 409

Soida M., Urbanik M., Beck R., Wielebinski R., 1999, A&A 345, 461

Tabara H., Inoue M., 1980, A&AS 39, 379

Thornley M.D., 1996 ApJ 469, 45

Thornley M.D., Mundy L.G., 1997, ApJ 484, 202

Tully R.B., 1988, Nearby Galaxies Catalog. Cambridge Univ. Press

Urbanik M., Beck R., Klein U., Gräve R., 1989, Ap&SS 156, 195

Urbanik M., Elstner D., Beck R., 1997, A&A 326, 465